



WPT TEST REPORT

No. 24T04Z100905-018

For

OnePlus Technology (Shenzhen) Co., Ltd.

Tablet

Model Name: OPD2403

with

Hardware Version: 88666_1_11

Software Version: OPD2403_14.1.0

FCC ID: 2ABZ2-OPD2403

Issued Date: 2024-06-18

Note:

The test results in this test report relate only to the devices specified in this report. This report shall not be reproduced except in full without the written approval of CTTL.

The report must not be used by the client to claim product certification, approval, or endorsement by NVLAP, NIST, or any agency of the U.S. Government.

Test Laboratory:

CTTL, Telecommunication Technology Labs, CAICT

No. 52, Huayuan North Road, Haidian District, Beijing, P. R. China 100191.

Tel:+86(0)10-62304633-2512, Fax:+86(0)10-62304633-2504

Email: ctl_terminals@caict.ac.cn, website: www.caict.ac.cn

**REPORT HISTORY**

Report Number	Revision	Issue Date	Description
24T04Z100905-018	Rev.0	2024-06-11	Initial creation of test report
24T04Z100905-018	Rev.1	2024-06-14	Update the information on page 7. Update the information for MAGPy on page 17.
24T04Z100905-018	Rev.2	2024-06-18	Update the information on page 17. Update the information for probe on page 29.

TABLE OF CONTENT

1 TEST LABORATORY	4
1.1. INTRODUCTION & ACCREDITATION	4
1.2. TESTING LOCATION	4
1.3. TESTING ENVIRONMENT	4
1.4. PROJECT DATA	4
1.5. SIGNATURE	4
2 CLIENT INFORMATION	5
2.1 APPLICANT INFORMATION	5
2.2 MANUFACTURER INFORMATION	5
3 EQUIPMENT UNDER TEST (EUT) AND ANCILLARY EQUIPMENT (AE)	6
3.1 ABOUT EUT	6
3.2 INTERNAL IDENTIFICATION OF EUT USED DURING THE TEST	6
3.3 INTERNAL IDENTIFICATION OF AE USED DURING THE TEST	6
4 APPLICABLE MEASUREMENT STANDARDS	6
5 INTRODUCTION	6
6 PRODUCT INFORMATION	7
7 SIMULATION TOOL AND MODEL	10
7.1 SIMULATION TOOL	10
7.2 MESH AND CONVERGENCE CRITERIA	10
7.3 POWER LOSS DENSITY CALCULATION	11
7.4 3D MODEL	11
8 SAR SIMULATION STEP	12
8.1 SIMULATIONS METHODOLOGY	12
8.2 H-FIELD STRENGTH MEASUREMENT AND SIMULATIONS	13
8.3 SAR SIMULATION	16
8.4 CALCULATION	17
9 MAIN TEST INSTRUMENTS	17
ANNEX A: TEST RESULT	18
ANNEX B: SPECIFIC INFORMATION FOR SAR COMPUTATIONAL MODELLING	19
ANNEX C: PROBE CALIBRATION CERTIFICATE	29
ANNEX D: ACCREDITATION CERTIFICATE	55

1 Test Laboratory

1.1. Introduction & Accreditation

Telecommunication Technology Labs, CAICT is an ISO/IEC 17025:2017 accredited test laboratory under American Association for Laboratory Accreditation (A2LA) with lab code 7049.01, and is also an FCC accredited test laboratory (CN1349), and ISED accredited test laboratory (CAB identifier:CN0066). The detail accreditation scope can be found on A2LA website.

1.2. Testing Location

Location 1: CTTL(huayuan North Road)

Address: No. 52, Huayuan North Road, Haidian District, Beijing,
P. R. China 100191

1.3. Testing Environment

Normal Temperature: 15-35°C
Extreme Temperature: -10/+55°C
Relative Humidity: 20-75%

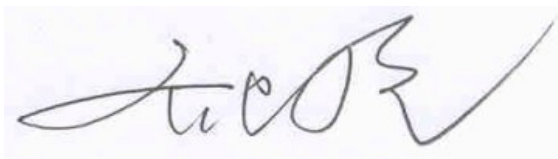
1.4. Project data

Testing Start Date: 2024-05-25
Testing End Date: 2024-06-08

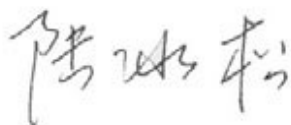
1.5. Signature



Wang Meng
(Prepared this test report)



Qi Dianyuan
(Reviewed this test report)



Lu Bingsong
Deputy Director of the laboratory
(Approved this test report)



2 Client Information

2.1 Applicant Information

Company Name:	OnePlus Technology (Shenzhen) Co., Ltd.
Address/Post:	18C02, 18C03, 18C04, and 18C05, Shum Yip Terra Building, Binhe Avenue North, Futian District, Shenzhen, Guangdong, P.R. China.
Contact Person:	Ariel Cheng
E-mail:	ariel.cheng@oneplus.com
Telephone:	(86)75561882366
Fax:	/

2.2 Manufacturer Information

Company Name:	OnePlus Technology (Shenzhen) Co., Ltd.
Address/Post:	18C02, 18C03, 18C04, and 18C05, Shum Yip Terra Building, Binhe Avenue North, Futian District, Shenzhen, Guangdong, P.R. China.
Contact Person:	Ariel Cheng
E-mail:	ariel.cheng@oneplus.com
Telephone:	(86)75561882366
Fax:	/

3 Equipment Under Test (EUT) and Ancillary Equipment (AE)

3.1 About EUT

Description:	Tablet
Model name:	OPD2403
Operating mode(s):	Wireless Charging
Operating Frequency:	110–148 kHz
Test device production information:	Production unit
Device type:	Portable device
Antenna type:	Integrated antenna
Hotspot mode:	Support

3.2 Internal Identification of EUT used during the test

EUT ID*	IMEI/SN	HW Version	SW Version
EUT1	W621521000006E3U900931	88666_1_11	OPD2403_14.1.0

*EUT ID: is used to identify the test sample in the lab internally.

3.3 Internal Identification of AE used during the test

AE ID*	Description	Model	SN	Manufacturer
AE1	Battery	BLT009	/	Sunwoda Electronic Co., Ltd.

*AE ID: is used to identify the test sample in the lab internally.

4 Applicable Measurement Standards

KDB 680106 D01 Wireless Power Transfer v04

TCB Workshop April 2024: Part 18 & Wireless Power Transfer

5 Introduction

This report demonstrates RF exposure compliance using SAR simulation for WPT of Tablet.

The device is a transmitter wireless charging device. The DUT can provide wireless charging for a handwriting pen. According to §2.1093 (certification for portable devices below 4 MHz), the device operating at 110-148 kHz should demonstrate RF exposure compliance to the 1.6 W/kg localized 1-g SAR limit. Therefore, to be conservative, we consider the device to be a portable device as a wireless charger. For portable devices, an accurate SAR value for the WPT transmitter is required. Since SAR test tools is not suitable for use below 100 MHz, we apply SAR numerical modeling to obtain SAR values.

The following sections describe the modeling, measured H-field, simulated H-field, and simulated SAR.

6 Product Information

This is a device supporting wireless charging function. It can provide charging for a handwriting pen through wireless charging. The Wireless power transfer application details are as below:

A. Wireless charging operating frequency

ANS: The wireless charging operating frequency range of the DUT is 110 kHz-148 kHz. The specific working frequency is 140 kHz.

B. Wireless charging maximum output power

ANS: When the DUT is used as the wireless charging Tx device, the maximum power of the wireless charging is 5 W.

C. Wireless charging usage scenarios

ANS: The device is a transmitter wireless charging device. The DUT can provide wireless charging for a handwriting pen. The DUT is used as a wireless charging transmitter device (Tx) in this usage scenario like Figure 1. The transmission system consists of coils and magnets. The device only supports one to one pairing with the client device.

It is automatically turn on the wireless charging Tx function when a handwriting pen placed directly in contact with the charging area of Tx device.



Figure 1. DUT Used as a wireless charging transmitter device

D. Wireless charging standard and operating diagram

ANS: The operating diagram of the wireless charging DUT is as below picture:

The adapter supplies power to the transmitter side and converts AC to DC by protocol. The transmitter converts DC to AC by using the LC charge/discharge circuit, which provides the transmitter coil to generate a magnetic field. The receiving coil couples AC power within the magnetic field, and provides it to the RX chip. The RX uses the rectifier output DC to achieve charging.

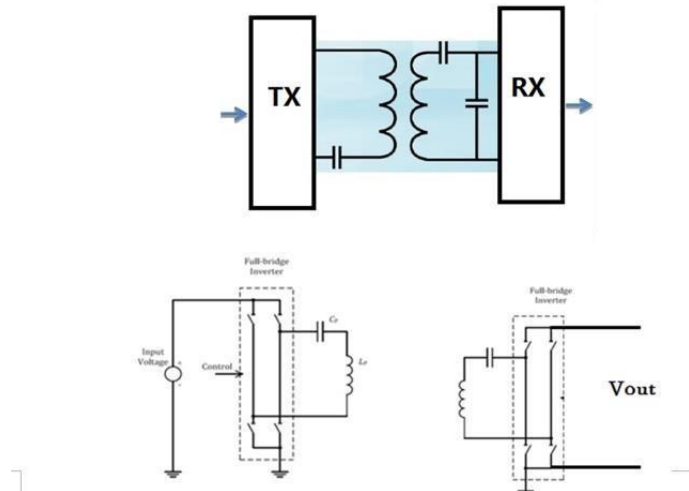


Figure 2. The wireless charging operating diagram

E. The number of turns for the primary coils, the amperes into the coil.

ANS: The device has a coil with 35 turns. The coil in DUT has 0.329A current while the DUT is operating in maximum output power.

F. Details on how charging is initiated and managed.

ANS: When the charging function (Tx mode) is enabled:

1. The wireless charging IC is powered on, and identifying the adapter type.
2. Then the PING frequency, the PING duration and the PING interval time are set.
3. The OCP (over current protection) and OVP (over voltage protection) parameters are set, the PING signal is sent, and the transmission is continued.
4. Once the PING is successful, the transmitting adjusts the transmission frequency according to the CEP (Control Error Packet) packet sent by the RX to establish a wireless power transmission.
5. Once RX is removed, TX re-enters the PING phase.

G.Detail information of the RF exposure analysis the coil design to simulate the actual coil.

ANS: The coil module is composed of a coil and a magnet with ferrite material, and the coil is wound around the magnet.

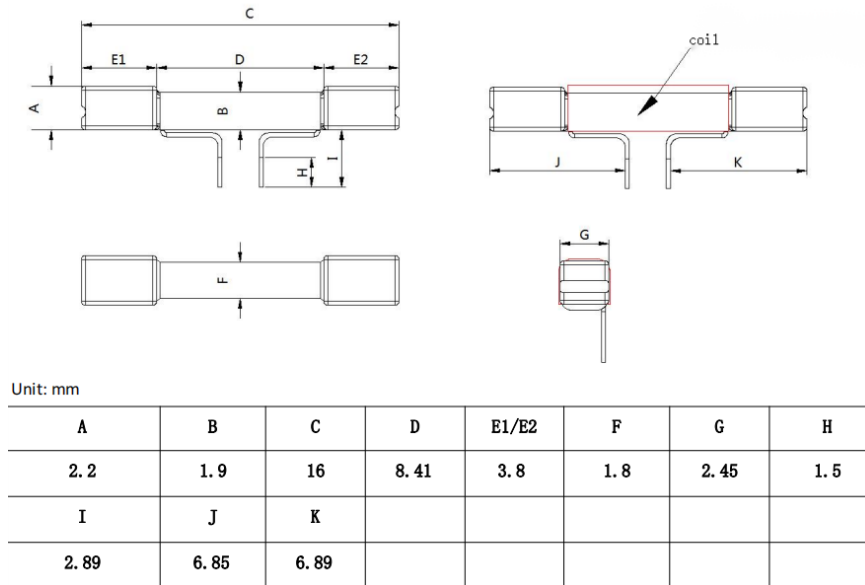


Figure 3. Coil Schematic

H.Description on the message exchanges between the transmitter and the receiver

ANS: Tx and Rx communicate using a single channel, and all Rx-Tx and Tx-Rx communication physical channels are wireless signals transmitted. Rx-Tx is ASK (Amplitude Shift Keying) communication, and Tx-Rx is FSK (Frequency-shift keying) communication. During the handshake, Rx sends a Signal Strength Packet, ID Packet, and Config Packet to the Tx. After the handshake is successful, Rx sends RPP (Received Power Packet) and CEP (Control Error Packet) to adjust the power.

7 Simulation Tool and Model

7.1 Simulation Tool

For the calculation of the magnetic field value and RF exposure simulation method of the EUT with the function of wireless charging, this article uses the electromagnetic module in SEMCAD. SEMCAD is one of several commercial tools for 3D electromagnetic simulation of wireless charging. The low frequency domain solver in SEMCAD is based on finite difference time domain (FDTD) solution.

7.2 Mesh and Convergence Criteria

To use FDTD to calculate the magnetic field value and RF exposure value of wireless charging, it is necessary to divide the charging device, human tissue, and surrounding environment into multiple small units. The physical quantities on the nodes and edges of each small unit can be used as the calculated magnetic field value and the process of dividing the unknown value into small cells is called meshing. In order to calculate the objective of the solution, the SEMCAD adaptive meshing technique was used. SEMCAD generates an initial mesh based on the minimum value of the wavelength of the electromagnetic field and the size of the target body, calculates the energy error during each iteration, and performs adaptive refinement and refinement for the regions with large errors. The determination of the number of calculation iterations in SEMCAD and the completion of the final iterative calculation process are called the convergence process. The convergence criterion tolerance is used to judge whether the convergence process is over. During the calculation process, the iterative adaptive grid process is performed until the convergence criterion tolerance is met. In SEMCAD, the accuracy of the convergence results depends on the tolerance. Figure 4 is an example of computing an object adaptive mesh.

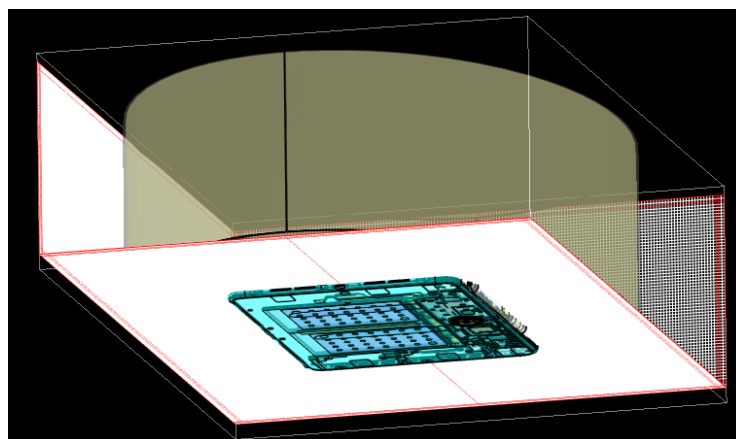


Figure 4. mesh generation of the model

7.3 Power Loss Density Calculation

By solving the three-dimensional wireless charging reverse charging simulation model, the numerical values of the electric field and magnetic field physical quantities at each position in the space can be obtained. In order to calculate the power density, two physical quantities need to be extracted: the electric field (\vec{E}) and the magnetic field (\vec{H}). The actual power density dissipated as the complex conjugate product of the electric field E and the magnetic field H yields the real part of the vector (\vec{S}) as follows:

$$\vec{S} = \frac{1}{2} \text{Re}(\vec{E} \times \vec{H})$$

\vec{S} is the power density at the node is calculated for each mesh, which can be obtained directly from SEMCAD.

From the point power density \vec{S} , the calculation formula of the average power density of the space volume V is as follows:

$$P = \frac{1}{V} \iiint \vec{S} \cdot dV$$

Here, the spatial average power density P is the total power density value of the x , y , and z components of the point power density, and the estimated volume is 1 cm^3 .

7.4 3D Model

Figure 5 shows the 3D simulation model of wireless charging device. The simulation model includes most of the finishing structure of the device: PCB, plastic frame, metal structure, wireless charging coil and magnetic conductive material, etc. It is often necessary to simplify, omit or substitute certain aspects of the EUT model to reduce simulation times and accommodate memory limitations. The model omits the foam support frame, glue, and the small component structure at the bottom of the tablet computer far from the charging coil. These parts have minimal impact on exposure assessment.

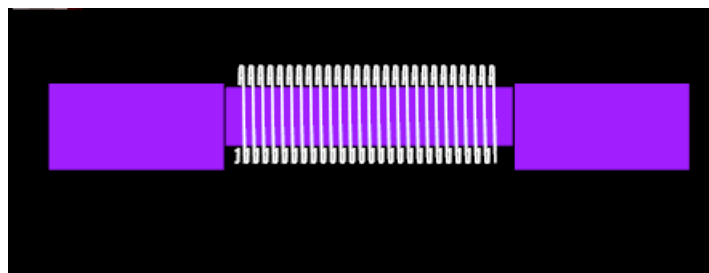


Figure 5. The 3D simulation model of wireless charging coil

8 SAR Simulation Step

8.1 Simulations Methodology

First, the CAD model of the wireless charging device is imported into the software for material definition and mesh division. Then the excitation signal type and the current were loaded into the model. And then, the electromagnetic model is excited by the current, and the simulated value of the field strength can be obtained. The accuracy of the wild goose array simulation is compared by the simulation and the actual measurement, and finally the RF exposure value is simulated.

8.1.1 Boundary Conditions

FDTD-based electromagnetic simulation tools need to impose boundary conditions on the simulation model, and the boundary conditions imposed are the first type of boundary conditions (Dirichlet boundary conditions). SEMCAD supports the direct application of Dirichlet boundary conditions.

8.1.2 Source Excitation Condition

The excitation conditions for wireless charging calculation are obtained by the circuit. The current can be applied directly at the coil port. After completing a 3D full-wave electromagnetic simulation of the modeled structure, the current to the coil can be loaded using the SEMCAD "low frequency source" function. Since SEMCAD uses a FDTD solver based on the frequency domain analysis method, the input source of the coil excitation is calculated using a sine signal for the operating frequency.

8.1.3 Simulation Completion Conditions

The simulation completion condition in SEMCAD is defined as a tolerance smaller than the desired value. The simulation result for this report is to set the tolerance to 1e-6.

8.2 H-field Strength Measurement and Simulations

We use the MAGPy to measure the actual H-field strength of the EUT. MAGPy has been designed for accurate measurements of both electric (0.08 V/m – 2000 V/m) and magnetic (0.1 – 3200 A/m) fields in the frequency range 3 kHz to 10 MHz. Both the field sensors and the electronic measuring circuitry are accommodated in a robust housing. Measurements are given total value (peak and average), with exceptional flatness and linearity. The probe specifications of H-field mode are giving below:

Table 1 The information of MAGPy for H-field measurement

Frequency range	3 kHz-10 MHz
Probe	8 isotropic H-field sensors (loop: 1 cm ² ; arranged at the corners of a cube of 22 mm side length)
Lowest H-field sensors	7.5 mm from the flat tip
H-field dynamic range	0.1 – 3200 A/m, 0.12 μ T – 4 mT
H-field gradient range	0 – 80 T/m/T
Temperature range	0 °C – 35 °C
Software	V2.6+

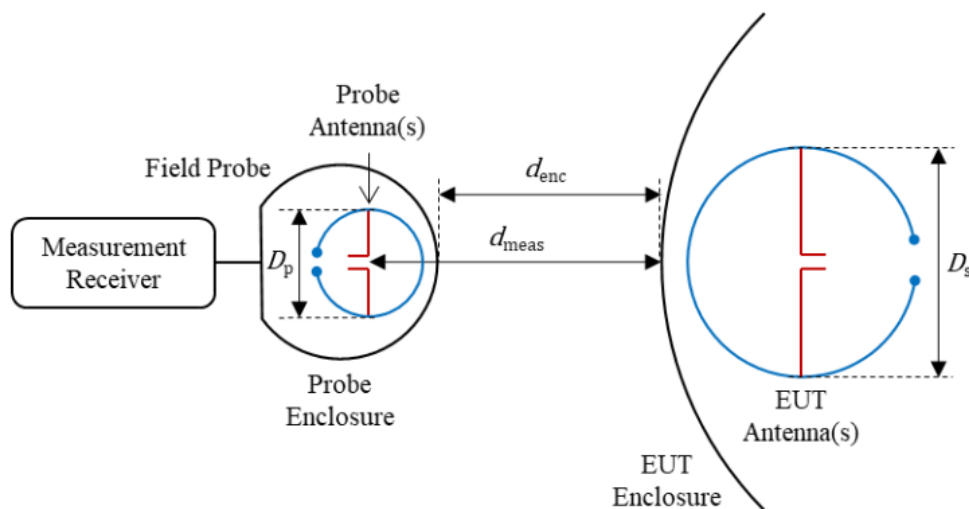


Figure 6. The located of sensitive element

The enclosure distance, denoted by d_{enc} in Figure is the distance between the EUT and the nearest surface of the field probe enclosure. The separation distance, d_{sep} , is the minimum distance between the EUT and the nearest surface of the exposure region (i.e. the region over which RF exposure is to be evaluated). The shortest distance separating the probe and EUT, denoted by d_{meas} in figure 6. Ideally, incident field measurements would be performed at the corresponding separation distance (i.e. $d_{meas} = d_{sep}$).

For the MAGPy the sensitive element is located approximately 7.5 mm below the external surface. When comparing the simulated values, the simulated field strength should be obtained at 7.5 mm from the surface of the EUT. The MAGPy is the only used for coils greater than 100mm. Therefore, the RF exposure was evaluated using a combination of simulation and testing.

When the charging device is close to the EUT device, the is activated. Start testing the EUT when operating at maximum transmit power. The front, back, left, right, top and bottom sides of the test are defined as shown in Figure 7.

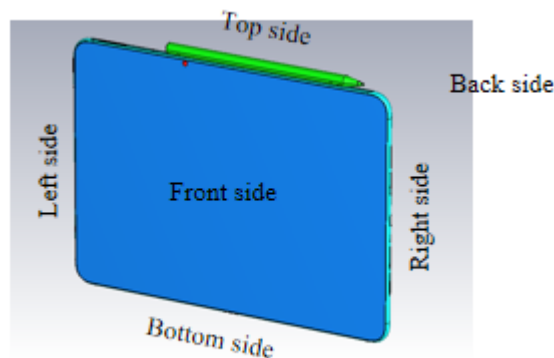


Figure 7. EUT test diagram

To accurately measure the value of the magnetic field strength, We measure the magnetic field values at different distances, and the test surface is the Front, Back, Right, Left, Top and Bottom sides that conform to the Portable device. Each point is repeat measured three times. See Annex A for the specific test results. The magnetic field is at its maximum when the tablet is at 90% power. Therefore, the test values are used to compare with the simulation results.

The H-field simulations are conducted using commercially available software SEMCAD. To validate the simulation model, H-field measurements are made on the EUT and compared to the simulated results (as shown in Figure 8). The validated model is then used for nerve stimulation simulations.

For wireless charging, the maximum transmit power of Tx is 5W. Although the conditions for this scenario are very harsh, considering the worst case, it needs to be simulated. The measured result and simulation result are shown below. It can be seen that the biggest gap between simulation and test is only 21.3%, which is far below the requirement of 30% . In this case the H-field strength values of the four sides are in good agreement with the simulated values. So, this mode can be used to calculate RF exposure.

Table 2. The Test and simulation result of H-field at 5W

Test/simulation Side	Test	Test Tx Power (W)	denc-test (mm)	Test Result (A/m)	Simulation Result (A/m)	Gap (%)
	Channel/Freq (kHz)					
Front Side	140	5	0	3.29	2.96	10.0%
Back Side	140	5	0	1.62	1.36	16.0%
Left Side	140	5	0	/	/	/
Right Side	140	5	0	/	/	/
Top Side	140	5	0	0.89	0.70	21.3%
Bottom Side	140	5	0	/	/	/

We did a simulation test comparison from 7.5 mm (the distance between the magnetic induction unit from the EUT surface) to 12 cm on the front side surface of 5 W. The results are shown in the following figure. The figure shows good correlation between the measurements and simulations.

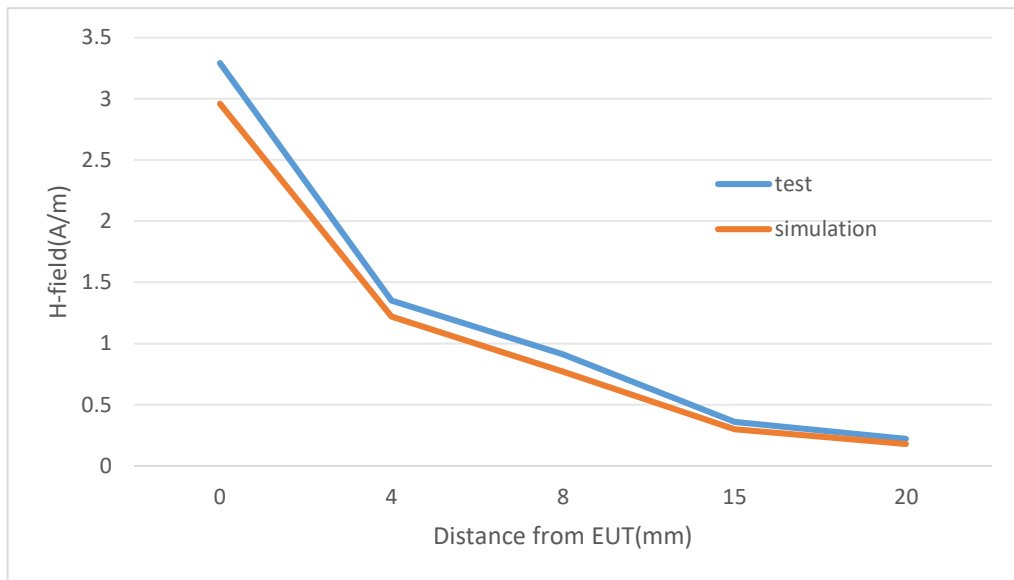


Figure 8. Comparison of test and simulation at different distances at 5 W

8.3 SAR simulation

The SAR simulations are conducted using commercially available software CST STUDIO SUITE by same model. For this simulation, a phantom is added in contact with the DUT.

The following steps are used for accurate SAR simulation:

- 1) Homogenous tissue material is used as liquid for desired frequency.
- 2) Power loss in phantom is calculated.
- 3) SAR can be calculated by the Equation:

$$SAR = \frac{P}{\rho}$$

where P is the Power loss density, and ρ is the tissue density.

- 4) SAR is averaged over 1 g at 0 mm.

The portable scene during charging appears when holding the DUT to use or placing it on the body to use the DUT. Therefore, it is necessary to determine the electrical properties of phantom. As mentioned earlier, the frequency of wireless charging is 140 kHz, so the electrical characteristics of the body and hand at this frequency are summarized as follows:

Table 3. The electrical characteristics for body layers

Property	Symbol	Value
Dielectric constant	ϵ_r	55(-)
Electrical conductivity	σ	0.75 S/m
Mass density	ρ	1000 kg/m ³

The phantom thickness is 150 mm. And the SAR results are peak spatial 1-gram average SAR.

The worst use case is at 5 W, we made SAR simulations for the 5W case without horizontal offset(Front side). The results are shown below:

SAR plot is show below (Front side without offset).

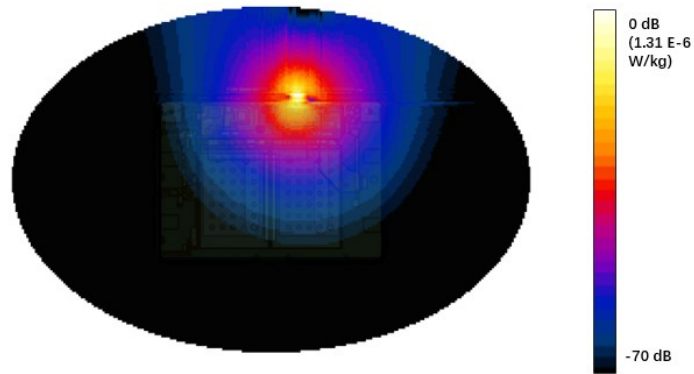


Figure 9. SAR distribution for front side without offset.

8.4 Calculation

The accuracy of the SAR simulations is demonstrated by correlating H-field measurements to simulations in Figure 9 and Table 2. For the case where the phones have no Horizontal offset, the highest peak spatial 1-g average SAR is 1.31×10^{-6} W/kg, well below SAR limit 1.6 W/kg.

9 MAIN TEST INSTRUMENTS

	Name	Type	SW Version	Serial Number	Calibration Date	Valid Period
01	Electromagnetic field probe	MAGPy-8H3D+E3D V2 MAGPy-DAS	2.6.0	3080/3076	Novberr 15, 2023	One year

Annex A: test result

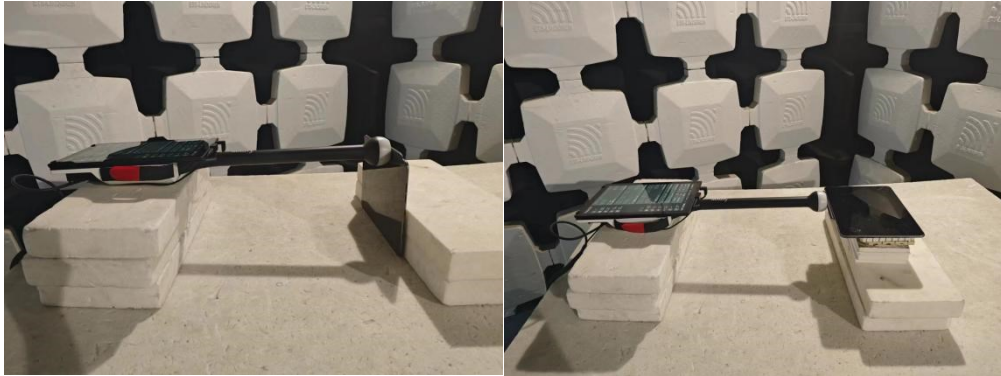


Figure 10. Test environment

Table 4. Magnetic field test results for different power levels of the plates

Tablet power-20%			Tablet power-50%			Tablet power-90%			
Position	Distance (mm)	test (A/m)	Position	Distance (mm)	test (A/m)	Position	Distance (mm)	test (A/m)	simulation (A/m)
Front Side	0	3.01	Front Side	0	3.07	Front Side	0	3.29	2.96
Front Side	4	1.2	Front Side	4	1.22	Front Side	4	1.35	1.22
Front Side	8	0.79	Front Side	8	0.84	Front Side	8	0.91	0.77
Front Side	15	0.28	Front Side	15	0.29	Front Side	15	0.36	0.3
Front Side	20		Front Side	20		Front Side	20	0.22	0.18
Back Side	0	1.35	Back Side	0	1.43	Back Side	0	1.62	1.36
Back Side	4	0.69	Back Side	4	0.66	Back Side	4	0.75	0.61
Back Side	8	0.4	Back Side	8	0.39	Back Side	8	0.45	0.4
Back Side	15		Back Side	15		Back Side	15	0.15	0.16
Top Side	0	0.79	Top Side	0	0.85	Top Side	0	0.89	0.7
Top Side	2	0.5	Top Side	2	0.48	Top Side	2	0.56	0.49
Top Side	5	0.29	Top Side	5	0.29	Top Side	5	0.38	0.33
Top Side	8		Top Side	8		Top Side	8	0.25	0.22

Annex B: specific information for SAR computational modelling

1) Computation Resources

The models were simulated on a 20-core-CPU server with an available RAM of 48 GB. Each model variation took around 0.5 hours to complete. Based on the simulation profile, the minimum resources needed to finish these simulations will be approximately 8 core CPU with 16 GB of RAM. Using the minimum requirements simulation will likely take more time than 2 hours.

2) Canonical benchmarks

All canonical benchmarks can be compared to analytical solutions of the physical problem or its numerical representation. These methods characterize the implementation of the FDTD algorithm in a very general way. They are defined such that it is not possible to tune the implementation for a particular benchmark or application without improving the overall quality of the code. The canonical benchmarks assess the cumulative accuracy of a code and its applicability considering the interaction of its different modules, such as mesh generation, computational kernel, representation of sources, data extraction algorithms of the post processor, etc.

All benchmarks of Canonical benchmarks shall be carried out with a three-dimensional implementation of the FDTD algorithm. Some benchmarks require the use of PEC, PMC or periodic boundary conditions.

3) Fundamentals of the FDTD method

The original algorithm introduced by Yee in 1966 forms the basis of the FDTD method where the electric and magnetic field components are positioned at the edges of a voxel and computed at alternate half time steps. Electromagnetic wave interactions in three-dimensions are solved with a system of six coupled partial differential equations. The resulting system of finite-difference equations requires only the adjacent field components from its previous time step to continue, and is highly adaptable to parallel processing.

The basic FDTD implementation is based on explicit, time staggered, and space staggered solution of discretized Maxwell's equations. For solutions in Cartesian coordinates, the field vectors E and H are dependent on the spatial variables x, y, z and the time variable t. The problem space is discretized into voxels $x = i\Delta x$, $y = j\Delta y$, $z = k\Delta z$, and time $t = n\Delta t$, where i, j and k are the voxel indices and n is the index of the time step. Using the central difference approximation for each field component, six explicit finite-difference equations are derived. It can be noted that the electric field components are staggered half a mesh step with respect to the magnetic field components. For instance, the magnetic field component, H_z at time $(n + 1/2)$ is computed from the value H_z at time $(n - 1/2)$ and the values of the electric fields at time n along the voxel edges forming the contour in the plane normal to H_z , namely: $E_{i+\frac{1}{2},j,k}^n$, $E_{i+\frac{1}{2},j+1,k}^n$, and $E_{i,j+\frac{1}{2},k}^n$, $E_{i+1,j+\frac{1}{2},k}^n$. Thus, Faraday's law is used to relate the line integral of the

electric field to the normal flux component of the magnetic field in the mesh. Likewise, Ampere's law is used to update the electric fields. The staggered space-time stepping solution of the Maxwell's curl equations is known as the leapfrog algorithm. Figure 11 shows the arrangement of the E- and H-field components. The algorithm consists of the so-called update equations for each electric field component and each magnetic field component. For the E_y - and the H_z -components, the update equations are written as:

$$E_{y,i,j+\frac{1}{2},k}^{n+1} = A_{y,i,j,k} E_{y,i,j+\frac{1}{2},k}^n + B_{x,i,j,k} \left(H_{x,i,j+\frac{1}{2},k+\frac{1}{2}}^{n+1/2} - H_{x,i,j+\frac{1}{2},k-\frac{1}{2}}^{n+1/2} \right) - B_{z,i,j,k} \left(H_{z,i+\frac{1}{2},j+\frac{1}{2},k}^{n+1/2} - H_{z,i-\frac{1}{2},j+\frac{1}{2},k}^{n+1/2} \right) \quad (1)$$

$$H_{z,i+\frac{1}{2},j+\frac{1}{2},k}^{n+1/2} = H_{z,i+\frac{1}{2},j+\frac{1}{2},k}^{n-1/2} + C_{y,j} \left(E_{y,i+\frac{1}{2},j+1,k}^n - E_{y,i+\frac{1}{2},j,k}^n \right) - C_{x,i} \left(E_{x,i+1,j+\frac{1}{2},k}^n - E_{x,i,j+\frac{1}{2},k}^n \right) \quad (2)$$

The coefficients of these equations, the so-called update coefficients, are given as:

$$A_{y_{i,j,k}} = \left(1 - \frac{\tilde{\sigma}_{y_{i,j,k}} \Delta t}{2\tilde{\varepsilon}_{y_{i,j,k}}} \right) / \left(1 + \frac{\tilde{\sigma}_{y_{i,j,k}} \Delta t}{2\tilde{\varepsilon}_{y_{i,j,k}}} \right) \quad (3)$$

$$B_{x_{i,j,k}} = \left(\frac{\Delta t}{\tilde{\varepsilon}_{y_{i,j,k}} \Delta z_k} \right) / \left(1 + \frac{\tilde{\sigma}_{y_{i,j,k}} \Delta t}{2\tilde{\varepsilon}_{y_{i,j,k}}} \right) \quad (4)$$

$$B_{z_{i,j,k}} = \left(\frac{\Delta t}{\tilde{\varepsilon}_{y_{i,j,k}} \Delta x_i} \right) / \left(1 + \frac{\tilde{\sigma}_{y_{i,j,k}} \Delta t}{2\tilde{\varepsilon}_{y_{i,j,k}}} \right) \quad (5)$$

$$C_{x_i} = \frac{\Delta t}{\mu_0 \Delta y_j} \quad (6)$$

$$C_{y_i} = \frac{\Delta t}{\mu_0 \Delta x_i} \quad (7)$$

It should be noted that this formulation includes no magnetic losses and the permeability of free space is μ_0 throughout the computational domain. Alternatively, the update coefficients can be derived based on the approach described as exponential time stepping.

ε and σ are the effective permittivity and conductivity of the mesh edges of the respective E-field components. They are calculated by averaging the dielectric properties of the surrounding voxels. Figure 12 shows an E_y -component in the FDTD mesh surrounded by voxels with four different dielectrics. ε and σ for the update equation of this component are calculated as

$$\tilde{\varepsilon}_y = \frac{\varepsilon_1 \Delta x_1 \Delta z_2 + \varepsilon_2 \Delta x_2 \Delta z_2 + \varepsilon_3 \Delta x_1 \Delta z_1 + \varepsilon_4 \Delta x_2 \Delta z_1}{(\Delta x_1 + \Delta x_2)(\Delta z_1 + \Delta z_2)} \quad (8)$$

$$\tilde{\sigma}_y = \frac{\sigma_1 \Delta x_1 \Delta z_2 + \sigma_2 \Delta x_2 \Delta z_2 + \sigma_3 \Delta x_1 \Delta z_1 + \sigma_4 \Delta x_2 \Delta z_1}{(\Delta x_1 + \Delta x_2)(\Delta z_1 + \Delta z_2)} \quad (9)$$

These definitions of ε and σ already consider variable mesh steps (see below). Expressions for the E_x - and E_z -components can be obtained by permuting the axis indices. The update coefficients of PEC edges shall be defined such that the electric field components on these edges are always kept at zero.

The time step for algorithm stability is given by the Courant condition or Courant, Friedrichs and Lewy (CFL) condition in Formula (10). For three-dimensional meshes with voxel edges of length Δx , Δy , Δz , and v as the maximum velocity of propagation in any medium in the problem, the time step size Δt is limited by

$$v \Delta t \leq \frac{1}{\sqrt{\frac{1}{(\Delta x)^2} + \frac{1}{(\Delta y)^2} + \frac{1}{(\Delta z)^2}}} \quad (10)$$

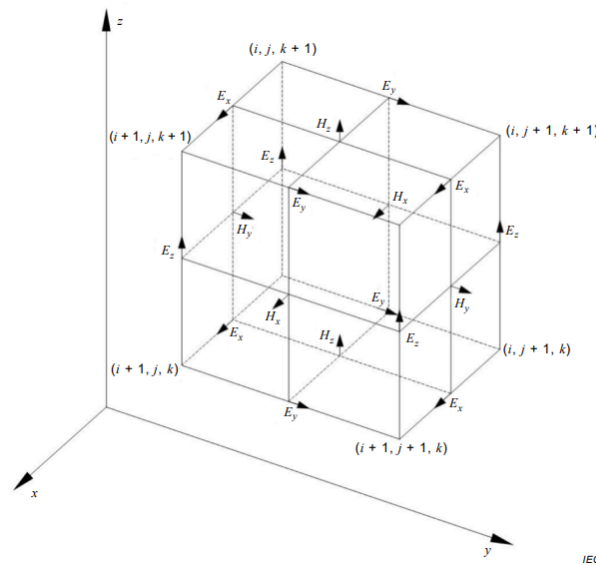


Figure 11 – Voxel showing the arrangement of the E- and H-field vector components on a staggered mesh

For variable meshes where Δx , Δy , Δz are functions of x , y , and z , respectively, the maximum time step for stability is obtained from considering the voxel which produces the smallest time step.

The phase velocity of numerical modes in the FDTD lattice can vary with modal wavelength, direction of propagation, and lattice discretization, causing dispersion of the simulated wave modes in the computational domain. This numerical dispersion can lead to nonphysical results such as pulse distortion, artificial anisotropy, and pseudo-refraction. The mesh size (Δx , Δy , Δz) typically is selected such that for the highest frequency at which the solution is valid, maximum $(\Delta x, \Delta y, \Delta z) \leq 0,1 \lambda$, where λ is the wavelength at that frequency in the most electrically dense penetrable material. This limits the numerical dispersion in most cases to an acceptable level. Under this condition, the error in the phase velocity of waves propagating in an arbitrary direction is not more than $-1,3 \%$. Thus, in this case, a sinusoidal numerical wave traveling a distance of only 2λ develops a lagging phase error of about $9,4^\circ$. This error is linearly cumulative with the wave propagation distance. Often the FDTD voxels in at least part of the mesh are much smaller than $0,1\lambda$ in order to accurately describe small geometry features.

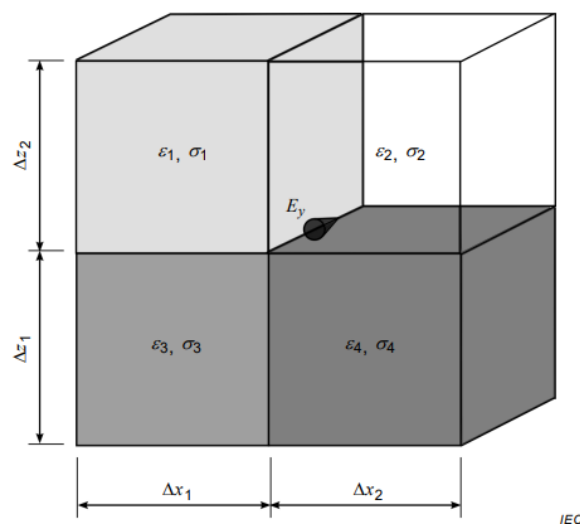


Figure 12 – Voxels with different dielectric properties surrounding a mesh edge with an E_y -component

4) Generic dipole

The feed-point impedance of a $\lambda/2$ -dipole (1 GHz) shall be evaluated for broadband excitation. If the software under test provides a harmonic simulation mode, the evaluation shall be carried out additionally in harmonic mode at 1 GHz. The dipole has a length of 150 mm and a diameter of 4 mm. The feeding gap size is 2 mm. The mesh shall be truncated with absorbing boundary conditions at 200 mm distance to the dipole in all directions. A broadband simulation covering the frequency range from 0,5 GHz to 1,5 GHz shall be performed. The radiated power shall be derived from the broadband simulation at 0,5 GHz, 1,0 GHz and 1,5 GHz. Reference results were derived with the method of moments. The homogeneous mesh has a step size of 2 mm. The minimum step of the inhomogeneous mesh is 1 mm (half of the feeding gap size) and the maximum step is 10 mm.

The quantities for evaluation and the maximum permitted error are given in Table 5.

Table 5 – Results of the dipole evaluation

Quantity	Simulation result (Homogeneous mesh)	Simulation result (Inhomogeneous mesh)	Tolerance
Re Z at 1 GHz	109.24	114.39	$40 \Omega < \text{Re } Z < 140 \Omega$
Im Z at 1 GHz	46.15	52.34	$30 \Omega < \text{Im } Z < 130 \Omega$
Frequency for Im Z = 0	909.76	894.14	$850 \text{ MHz} < f < 950 \text{ MHz}$
Power budget at 0,5 GHz	0.08	1.21	< 5 %
Power budget at 1,0 GHz	0.08	1.18	< 5 %
Power budget at 1,50 GHz	0.07	1.16	< 5 %

5) Microstrip terminated with ABC

The propagation constant and wave impedance of a micro strip line and the reflection coefficient for quasi-TEM operation shall be evaluated. The micro strip has a characteristic impedance of 50Ω . The substrate is lossless and has a relative permittivity of 3,4. The geometry of the strip line is given in Figure 13. For an impedance of 50Ω , the width w of the strip line and the height h of the substrate shall be 2,8 mm and 1,2 mm, respectively.

The strip line shall be modelled in an inhomogeneous mesh with a minimum step size of 0,1 mm and a maximum step size of 1 mm. The thickness of the microstrip is negligible with respect to the other dimensions of the geometry. It can therefore be meshed as an infinitely thin sheet. Special techniques for the representation of thin sheets can be applied, but shall be validated, and their modifications to the update coefficients or the Yee algorithm shall be documented. The microstrip shall be evaluated with its orientation aligned with the mesh. The strip line shall be terminated with ABCs. For the excitation, a broadband signal shall be used covering the frequency range from 0,5 GHz to 2,0 GHz. As a source, a single edge can be used or the quasi-TEM mode can be excited directly. The voltages and currents on the strip line shall be recorded at three points along the strip line in 30 mm distance from one another. The distance of the first of these points to the source shall be at least 30 mm. A sufficient distance between the source and the recording locations shall be kept in order to avoid the coupling of spurious components into the voltage and current sensors. When calculating the wave impedance, the phase offset between the voltage and current due to the leapfrog scheme shall be considered. The results to be reported are summarized in Table 6. For all quantities, the maximum error over the frequency range from 0,5 GHz to 2,0 GHz shall be reported.

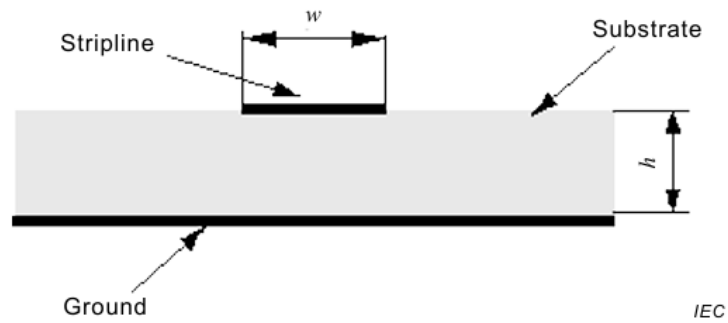


Figure 13 – Geometry of the microstrip line

Table 6 – Results of the microstrip evaluation

Results of the microstrip evaluation @ 0.5 GHz			
Quantity	Reference	Deviation	Tolerance
Re Z	50 Ω	48.5099 Ω	45 Ω < Re Z < 55 Ω
Im Z	0	-1.028e-13 Ω	-2 Ω < Im Z < 2 Ω
Reflection coefficient	$-\infty$ dB	-37.22 dB	< -20 dB

Results of the microstrip evaluation @ 2.0 GHz			
Quantity	Reference	Deviation	Tolerance
Re Z	50 Ω	48.3753 Ω	45 Ω < Re Z < 55 Ω
Im Z	0	-1.315e-12 Ω	-2 Ω < Im Z < 2 Ω
Reflection coefficient	$-\infty$ dB	-36.25 dB	< -20 dB

6) SAR calculation SAM phantom / generic phone

The benchmark described in Beard et al. shall be repeated for the SAM phantom with the generic phone in the “touch” and the “tilted” position (IEEE Std 1528) at 835 MHz and 1 900 MHz; 1 g and 10 g peak spatial-average SAR values shall be reported for the two positions and frequencies. The SAR results shall be normalized to the feed-point power, i.e. the accepted antenna power. They shall be within $\pm 50\%$ of the mean values reported by Beard et al. (Table 7), which corresponds to two times the reported standard deviation.

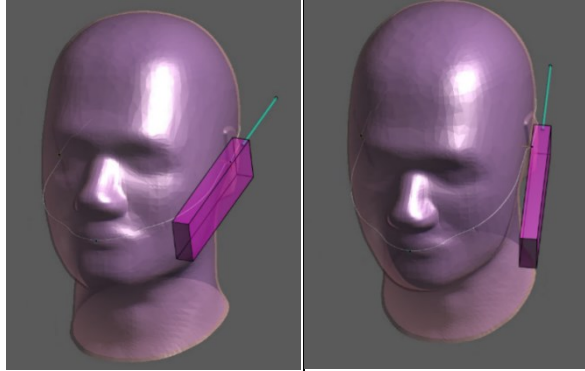


Figure 14 – the SAM phantom with the generic phone in the “touch” and the “tilted” position

Table 7 – 1 g and 10 g psSAR for the SAM phantom exposed to the generic phone for 1 W accepted antenna power

Quantity	835 MHz “touch”	835 MHz “tilted”	1900 MHz “touch”	1900 MHz “tilted”
1g psSAR by Beard et al [W/kg]	7.5	4.9	8.3	12.0
1g psSAR CTTL [W/kg]	8.681	4.361	7.378	9.643
Deviations (%)	16%	11%	11%	20%
10g psSAR by Beard et al [W/kg]	5.3	3.4	4.8	6.8
10g psSAR CTTL [W/kg]	6.221	3.179	4.774	5.565
Deviations (%)	17%	7%	1%	18%

7) Setup for system performance check

The dipole and flat phantom configuration for the system performance check defined in IEC 62209-1 and IEEE Std 1528 shall be simulated at 900 MHz and 3 000 MHz. using the dielectric parameters given in Table 8 and the dimensions given in Table 9 and Figure 15. The height of the tissue simulant above the phantom shell shall be 150 mm. The parameters are:

- f frequency of operation;
- ϵ_r relative permittivity of the tissue simulant;
- σ conductivity of the tissue simulant;
- t thickness of the phantom shell;
- d diameter of the rods of the dipole and of the $\lambda/4$ stub;
- l length of the dipole; h length of the $\lambda/4$ stub;
- s distance from the bottom of the tissue simulant to the centre axis of the dipole rods;
- w distance between the rods of the $\lambda/4$ stub;
- x length of the phantom (along the dipole axis);
- y width of the phantom;
- z height of the tissue simulant.

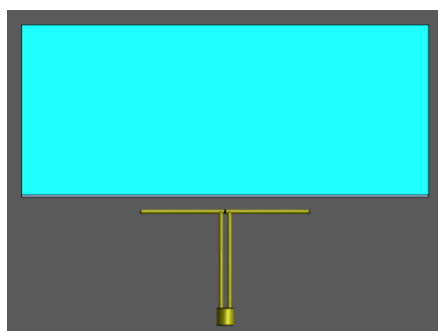
The 1 g and the 10 g peak spatial-average SAR and the feed-point impedance shall be evaluated. The deviation of the peak spatial-average SAR and the real part of the feed-point impedance from the values reported in Table 10 shall not be larger than $\pm 10\%$. The imaginary part of the feed-point impedance shall be within $\pm 5\ \Omega$. Details on the numerical evaluation of the setup for the system performance check can be found in Christ et al. research.

Table 8 – Dielectric parameters of the setup

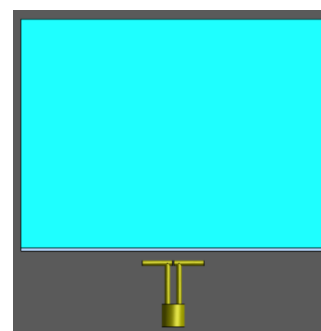
f [MHz]	tissue simulant		phantom shell	
	ϵ_r	σ [S/m]	ϵ_r	σ [S/m]
900	41,5	0,97	3,7	0
3000	38,5	2,4	3,7	0

Table 9 – Mechanical parameters of the setup

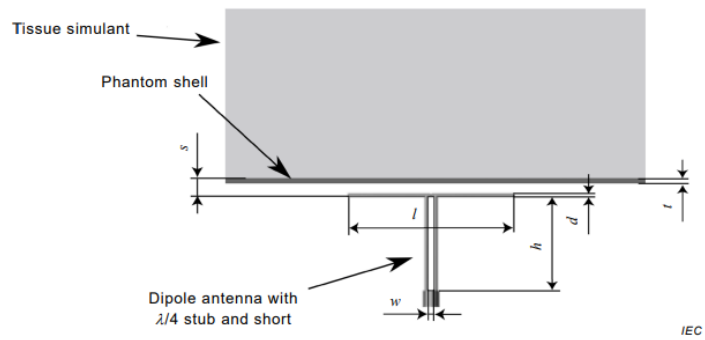
f [MHz]	t [mm]	d [mm]	l [mm]	h [mm]	s [mm]	w mm]	x [mm]	y [mm]	z [mm]
900	2,0	3,6	149,0	83,3	15,0	4,0	360,0	300,0	150,0
3 000	2,0	3,6	41,5	25,0	10,0	4,0	200,0	160,0	150,0



(a)



(b)



(c)

Figure 15 – Models and geometry of the setup for the system performance check according to Christ et al. research.

(a)900 MHz Model (b)3000 MHz Model

(c) Geometry of the setup for the system performance check according to Christ et al. research

Table 10 – psSAR normalized to 1 W forward power and feedpoint impedance

psSAR normalized to 1 W forward power and feedpoint impedance												
f (MHz)	1 g psSAR [W/kg]			10 g psSAR [W/kg]			Re Z [Ω]			Im Z [Ω]		
	CT TL	Christ, A	Deviations (%)	CT TL	Christ, A	Deviations (%)	CT TL	Christ, A	Deviations (%)	CT TL	Christ, A	Deviations (%)
900	10.72	11	-2.55%	6.85	7.07	-3.11%	51.17	49.9	2.55%	5.54	2.3	3.24 Ω
3000	61.57	65.4	-5.86%	24.69	25.3	-2.41%	50.398	53.4	-5.62%	-8.31	-4	-4.31 Ω

8) Total Computational Uncertainty

Below is a table summarizing the budget of the uncertainty contributions of the numerical algorithm and of the rendering of the simulation setup. The table was filled using the IEC 62704-1, 2020.

For the simulations, the extreme case where the phantom is placed directly in front of the tablet is considered.

Table 11. Budget of uncertainty contributions of the numerical algorithm (filled based on IEC 62704-1 2020).

a	b	d	e	g
Uncertainty component	Subclause	Probability distribution	Divisor $f(d, h)$	Uncertainty %
Mesh resolution	7.2.2	N	1	3.06
ABC	7.2.3	N	1	
Convergence	7.2.5	R	1,73	
Phantom dielectrics	7.2.6	R	1,73	
Combined standard uncertainty (k= 1)				3.06

Below is a table summarizing the budget of the uncertainty of the developed model of the EUT so far. The table was filled using the IEC 62704-1, 2020.

Table 12. Uncertainty of DUT Model

a	b	d	e	g
Uncertainty component	Subclause	Probability distribution	Divisor $f(d, h)$	Uncertainty %
Uncertainty of the DUT model (based on near field distribution)	7.3.2	N	1	2.3
Uncertainty of the measurement equipment and procedure	7.3.3	N	1	4
Combined standard uncertainty (k= 1)				6.3

Table 14. Expanded Standard Uncertainty

a	b	d	e	g
Uncertainty component	Subclause	Probability distribution	Divisor $f(d, h)$	Uncertainty %
Uncertainty of the test setup with respect to simulation parameters	7.2	N	1	3.06

Uncertainty of the developed numerical model of the test setup	7.3	N	1	6.3
Combined standard uncertainty (k= 1)				9.36
Expanded standard uncertainty (k= 2)				18.72

References:

- 1) IEC/IEEE 62704-1 (Edition 1.0 2017-10) Determining the peak spatial-average specific absorption rate (SAR) in the human body from wireless communications devices, 30 MHz to 6 GHz–Part 1: General requirements for using the finite-difference time-domain (FDTD) method for SAR calculations
- 2) IEC/IEEE 62704-4 (Edition 1.0 2020-10) Determining the peak spatial-average specific absorption rate (SAR) in the human body from wireless communications devices, 30 MHz to 6 GHz – Part 4:General requirements for using the finite element method for SAR calculations
- 3) Federal Communications Commission Office of Engineering and Technology Laboratory Division – 680106 D01 Wireless Power Transfer v04
- 4) RSS-102.NS.SIM Issue 1 December 15, 2023 – Simulation Procedure for Assessing Nerve Stimulation (NS) Compliance in Accordance with RSS-102

Annex C: Probe Calibration Certificate

Calibration Laboratory of
 Schmid & Partner
 Engineering AG
 Zeughausstrasse 43, 8004 Zurich, Switzerland



S Schweizerischer Kalibrierdienst
C Service suisse d'étalonnage
S Servizio svizzero di taratura
S Swiss Calibration Service

Accredited by the Swiss Accreditation Service (SAS)
 The Swiss Accreditation Service is one of the signatories to the EA
 Multilateral Agreement for the recognition of calibration certificates

Accreditation No.: **SCS 0108**

Client **Auden**
 Taoyuan City

Certificate No. **MAGPy-8H3D-3080**

CALIBRATION CERTIFICATE

Object **MAGPy-8H3D+E3D SN:3080**
MAGPy-DAS SN:3076

Calibration procedure(s) **QA CAL-46.v1**
Calibration Procedure for MAGPy-8H3D+E3D
Near-field Electric and Magnetic Field Sensor System

Calibration date **November 15, 2023**

This calibration certificate documents the traceability to national standards, which realize the physical units of measurements (SI).
 The measurements and the uncertainties with confidence probability are given on the following pages and are part of the certificate.

All calibrations have been conducted in the closed laboratory facility: environment temperature $(22 \pm 3)^\circ\text{C}$ and humidity $< 70\%$.

Calibration Equipment used (M&TE critical for calibration)

Primary Standards	ID	Cal Date (Certificate No.)	Scheduled Calibration
Oscilloscope	SN: 112135	25-Sep-23 (No. 17A1162175)	Sep-24
Reference 20 dB Attenuator	SN: CC2552 (20x)	04-Apr-23 (No. 217-03527)	Apr-24
Type-N mismatch	SN: 310982 / 06327	04-Apr-23 (No. 217-03528)	Apr-24

Secondary Standards	ID	Check Date (in house)	Scheduled Check
Network Analyzer E5061B	SN: MY49810822	In house check: Nov-22	In house check: Nov-23
TEM Cell	SN: S6029i	In house check: Nov-22	N.A
Plate Capacitor	SN: 6028i	In house check: Nov-22	In house check: Nov-23
Resonator (160kHz)	SN: 6030i	In house check: Nov-22	In house check: Nov-23

	Name	Function	Signature
Calibrated by	Aidonia Georgiadou	Laboratory Engineer	
Approved by	Sven Kühn	Technical Manager	

Issued: November 15, 2023

This calibration certificate shall not be reproduced except in full without written approval of the laboratory.

Calibration Laboratory of
Schmid & Partner
Engineering AG
Zeughausstrasse 43, 8004 Zurich, Switzerland



S Schweizerischer Kalibrierdienst
C Service suisse d'étalonnage
S Servizio svizzero di taratura
S Swiss Calibration Service

Accredited by the Swiss Accreditation Service (SAS)
The Swiss Accreditation Service is one of the signatories to the EA
Multilateral Agreement for the recognition of calibration certificates

Accreditation No.: **SCS 0108**

Glossary

MAGPy-8H3D-E3D Magnetic Amplitude and Gradient Probe – Eight H-field Sensors, Single E-field sensor
MAGPy-DAS Magnetic Amplitude and Gradient Data Acquisition System

Calibration is Performed According to the Following Standards:

- a) IEEE Std 1309-2013, "IEEE Standard for calibration of electromagnetic field sensors and probes, excluding antennas, from 9 kHz to 40 GHz", November 2013

Methods Applied and Interpretation of Parameters

- Calibration has been performed after the adjustment of the device.
- *Linearity*: Calibration of the linearity of the field reading over the specified dynamic range at 161.75 kHz. Influence of offset voltage is included in this measurement.
- *Frequency response*: Calibration of the field reading over the specified frequency range from 3.0 kHz to 10.0 MHz.
- Receiving Pattern: Assessed for H-field polarizations ϑ , and $\phi = 0^\circ \dots 360^\circ$; $\vartheta = 90^\circ$, and $\phi = 0^\circ \dots 360^\circ$; for the XYZ sensors (in TEM-Cell at 4 kHz, 40 kHz, 400 kHz and 4 MHz).
- Receiving Pattern: Assessed for E-field polarizations ϑ , and $\phi = 0^\circ \dots 360^\circ$; $\vartheta = 90^\circ$, and $\phi = 0^\circ \dots 360^\circ$; for the XYZ sensor (in parallel plate capacitor at 4 kHz, 40 kHz, 400 kHz and 4 MHz).

Calibration Uncertainty

The calibration uncertainty is 0.7 dB for the H-field readings and 1.06 dB for the E-field readings. The calibration uncertainty is specified over the frequency range from 3.0 kHz to 10.0 MHz and a dynamic range from 0.1 A/m to 3200 A/m and from 0.08 V/m to 2000 V/m respectively.

The reported uncertainty of measurement is stated as the standard uncertainty of measurement multiplied by the coverage factor $k=2$, which for a normal distribution corresponds to a coverage probability of approximately 95%.



MAGPy-8H3D+E3D SN:3080
 MAGPy-DAS SN:3076

November 15, 2023

Measurement Conditions

Unit Type	MAGPy-8H3D+E3D (SP MGY 303 AA)	3080
	MAGPy-DAS (SE UMS 303 AC)	3076
	MAGPy FPGA Board	WP000228
Adjustment Date	Last MAGPy Adjustment	November 15, 2023
Firmware SW Version	MAGPy Firmware	Ver. 1.00
Backend SW Version	MAGPy Backend	Ver. 1.0.2
Calibration SW Version	MAGACAP	Ver. 1.0

Dynamic Range

Dynamic Range, H-field, Channel 0

H-field/(A/m) Applied			H-field/(A/m) Reading			Difference/(dB)			Tolerance/(dB)
x	y	z	x	y	z	x	y	z	
0.400	0.390	0.370	0.420	0.370	0.400	0.42	-0.46	0.68	±1.00
0.540	0.530	0.510	0.560	0.530	0.510	0.32	0.00	0.00	±1.00
0.740	0.730	0.700	0.750	0.720	0.700	0.12	-0.12	0.00	±1.00
0.970	0.950	0.910	0.980	0.960	0.920	0.09	0.09	0.09	±1.00
1.31	1.28	1.23	1.31	1.28	1.23	0.00	0.00	0.00	±1.00
1.80	1.76	1.69	1.81	1.76	1.70	0.05	0.00	0.05	±1.00
2.39	2.35	2.25	2.41	2.35	2.25	0.07	0.00	0.00	±0.20
3.20	3.14	3.01	3.21	3.15	3.00	0.03	0.03	-0.03	±0.20
4.35	4.26	4.08	4.35	4.26	4.10	0.00	0.00	0.04	±0.20
5.88	5.77	5.52	5.90	5.77	5.54	0.03	0.00	0.03	±0.20
7.91	7.76	7.42	7.93	7.76	7.44	0.02	0.00	0.02	±0.20
10.6	10.4	9.91	10.6	10.4	9.93	0.00	0.00	0.02	±0.20
14.3	14.0	13.4	14.3	14.0	13.4	0.00	0.00	0.00	±0.20
19.2	18.9	18.1	19.2	18.8	18.1	0.00	-0.05	0.00	±0.20
26.0	25.5	24.4	25.9	25.5	24.4	-0.03	0.00	0.00	±0.20
34.7	34.0	32.6	34.8	34.2	32.7	0.02	0.05	0.03	±0.20
46.8	46.0	44.0	46.9	46.1	44.1	0.02	0.02	0.02	±0.20
63.4	62.2	59.6	63.6	62.4	59.8	0.03	0.03	0.03	±0.20
87.0	85.4	81.7	86.8	85.2	81.5	-0.02	-0.02	-0.02	±0.20
114	112	107	114	111	107	0.00	-0.08	0.00	±0.20
157	154	147	156	153	147	-0.06	-0.06	0.00	±0.20
217	213	204	217	213	204	0.00	0.00	0.00	±0.20
300	295	282	302	290	278	0.06	-0.15	-0.12	±0.20
444	435	417	438	430	412	-0.12	-0.10	-0.10	±0.20
612	601	575	608	597	572	-0.06	-0.06	-0.05	±0.20
912	896	857	916	900	862	0.04	0.04	0.05	±0.20
1380	1350	1300	1400	1380	1320	0.12	0.19	0.13	±0.30
1900	1860	1780	1950	1920	1830	0.23	0.28	0.24	±0.30
3070	3020	2890	3190	3140	3000	0.33	0.34	0.32	±0.50
3720	3650	3500	3880	3810	3660	0.37	0.37	0.39	±0.50

SPEAG H-field linearity tolerance criteria¹:
 ±1.0dB for applied H-fields < 2.0A/m
 ±0.2dB for applied H-fields ≥ 2.0A/m and < 1000A/m
 ±0.3dB for applied H-fields ≥ 1000A/m and < 2000A/m
 ±0.4dB for applied H-fields ≥ 2000A/m and < 3000A/m
 ±0.5dB for applied H-fields ≥ 3000A/m

¹ Calibration uncertainty not taken into account (shared risk 50%).



MAGPy-8H3D+E3D SN:3080
 MAGPy-DAS SN:3076

November 15, 2023

Dynamic Range, H-field, Channel 1

H-field/(A/m) Applied			H-field/(A/m) Reading			Difference/(dB)			Tolerance/(dB)
x	y	z	x	y	z	x	y	z	
0.400	0.390	0.390	0.410	0.420	0.410	0.21	0.64	0.43	±1.00
0.540	0.530	0.530	0.540	0.540	0.550	0.00	0.16	0.32	±1.00
0.740	0.730	0.720	0.730	0.720	0.730	-0.12	-0.12	0.12	±1.00
0.960	0.950	0.940	0.970	0.950	0.930	0.09	0.00	-0.09	±1.00
1.30	1.28	1.27	1.32	1.29	1.27	0.13	0.07	0.00	±1.00
1.79	1.76	1.75	1.80	1.76	1.75	0.05	0.00	0.00	±1.00
2.38	2.34	2.33	2.39	2.37	2.32	0.04	0.11	-0.04	±0.20
3.19	3.13	3.11	3.19	3.16	3.13	0.00	0.08	0.06	±0.20
4.32	4.25	4.23	4.33	4.27	4.23	0.02	0.04	0.00	±0.20
5.85	5.75	5.72	5.84	5.77	5.72	-0.01	0.03	0.00	±0.20
7.87	7.74	7.69	7.87	7.77	7.68	0.00	0.03	-0.01	±0.20
10.5	10.3	10.3	10.5	10.4	10.3	0.00	0.08	0.00	±0.20
14.2	14.0	13.9	14.2	14.0	13.9	0.00	0.00	0.00	±0.20
19.1	18.9	18.7	19.1	18.9	18.7	0.00	0.00	0.00	±0.20
25.8	25.4	25.2	25.8	25.4	25.2	0.00	0.00	0.00	±0.20
34.5	33.9	33.7	34.6	34.1	33.9	0.03	0.05	0.05	±0.20
46.6	45.9	45.5	46.7	46.0	45.7	0.02	0.02	0.04	±0.20
63.0	62.0	61.7	63.2	62.3	61.9	0.03	0.04	0.03	±0.20
86.5	85.2	84.7	86.3	84.9	84.4	-0.02	-0.03	-0.03	±0.20
113	112	111	113	111	111	0.00	-0.08	0.00	±0.20
156	153	152	155	153	152	-0.06	0.00	0.00	±0.20
216	213	211	215	212	211	-0.04	-0.04	0.00	±0.20
299	294	292	300	289	287	0.03	-0.15	-0.15	±0.20
442	434	432	435	429	427	-0.14	-0.10	-0.10	±0.20
608	599	596	604	595	592	-0.06	-0.06	-0.06	±0.20
907	894	888	911	898	892	0.04	0.04	0.04	±0.20
1370	1350	1340	1390	1370	1370	0.13	0.13	0.19	±0.30
1890	1860	1850	1940	1910	1900	0.23	0.23	0.23	±0.30
3060	3010	2990	3170	3130	3110	0.31	0.34	0.34	±0.50
3700	3640	3620	3860	3800	3780	0.37	0.37	0.38	±0.50

SPEAG H-field linearity tolerance criteria¹:

- ±1.0 dB for applied H-fields < 2.0 A/m
- ±0.2 dB for applied H-fields ≥ 2.0 A/m and < 1000 A/m
- ±0.3 dB for applied H-fields ≥ 1000 A/m and < 2000 A/m
- ±0.4 dB for applied H-fields ≥ 2000 A/m and < 3000 A/m
- ±0.5 dB for applied H-fields ≥ 3000 A/m

¹Calibration uncertainty not taken into account (shared risk 50%).

MAGPy-8H3D+E3D SN:3080
MAGPy-DAS SN:3076

November 15, 2023

Dynamic Range, H-field, Channel 2

H-field/(A/m) Applied			H-field/(A/m) Reading			Difference/(dB)			Tolerance/(dB)
x	y	z	x	y	z	x	y	z	
0.400	0.390	0.390	0.420	0.410	0.410	0.42	0.43	0.43	±1.00
0.550	0.530	0.530	0.550	0.550	0.530	0.00	0.32	0.00	±1.00
0.750	0.720	0.730	0.760	0.730	0.710	0.12	0.12	-0.24	±1.00
0.980	0.940	0.950	1.00	0.960	0.950	0.18	0.18	0.00	±1.00
1.32	1.28	1.28	1.35	1.30	1.30	0.20	0.13	0.13	±1.00
1.81	1.76	1.76	1.84	1.76	1.76	0.14	0.00	0.00	±1.00
2.42	2.34	2.35	2.44	2.36	2.35	0.07	0.07	0.00	±0.20
3.23	3.13	3.14	3.24	3.14	3.14	0.03	0.03	0.00	±0.20
4.39	4.25	4.26	4.41	4.25	4.26	0.04	0.00	0.00	±0.20
5.94	5.74	5.77	5.95	5.74	5.76	0.01	0.00	-0.02	±0.20
7.99	7.73	7.75	8.00	7.73	7.74	0.01	0.00	-0.01	±0.20
10.7	10.3	10.3	10.7	10.3	10.3	0.00	0.00	0.00	±0.20
14.4	13.9	14.0	14.4	13.9	14.0	0.00	0.00	0.00	±0.20
19.4	18.8	18.9	19.4	18.8	18.9	0.00	0.00	0.00	±0.20
26.2	25.4	25.5	26.2	25.4	25.5	0.00	0.00	0.00	±0.20
35.0	33.9	34.0	35.1	34.0	34.1	0.02	0.03	0.03	±0.20
47.3	45.8	45.9	47.4	45.9	46.1	0.02	0.02	0.04	±0.20
64.0	61.9	62.2	64.2	62.2	62.4	0.03	0.04	0.03	±0.20
87.8	85.0	85.3	87.6	84.8	85.1	-0.02	-0.02	-0.02	±0.20
115	111	112	115	111	111	0.00	0.00	-0.08	±0.20
158	153	154	158	153	153	0.00	0.00	-0.06	±0.20
219	212	213	219	212	213	0.00	0.00	0.00	±0.20
303	294	295	305	289	290	0.06	-0.15	-0.15	±0.20
448	434	435	442	428	430	-0.12	-0.12	-0.10	±0.20
618	598	600	613	595	597	-0.07	-0.04	-0.04	±0.20
921	892	895	924	896	899	0.03	0.04	0.04	±0.20
1390	1350	1350	1410	1370	1380	0.12	0.13	0.19	±0.30
1910	1860	1860	1960	1910	1910	0.22	0.23	0.23	±0.30
3100	3000	3020	3220	3120	3130	0.33	0.34	0.31	±0.50
3760	3640	3650	3910	3800	3810	0.34	0.37	0.37	±0.50

SPEAG H-field linearity tolerance criteria¹:

- ±1.0 dB for applied H-fields < 2.0 A/m
- ±0.2 dB for applied H-fields ≥ 2.0 A/m and < 1000 A/m
- ±0.3 dB for applied H-fields ≥ 1000 A/m and < 2000 A/m
- ±0.4 dB for applied H-fields ≥ 2000 A/m and < 3000 A/m
- ±0.5 dB for applied H-fields ≥ 3000 A/m

¹ Calibration uncertainty not taken into account (shared risk 50%).